 FDMP, vol.2, no.4, pp.261-269, 2006

A Numerical Study of Controlling The G-Jitter Induced Convection in The Solution of A Crystal Growth Crucible under Microgravity

Y. Okano[1], A. Ishii[1], H. Miyashita[1], H. Minakuchi[1] and S. Dost[2]

Abstract: The article presents the results of a numerical simulation study that was carried out to examine the effect of g-jitter on the flow and concentration structures observed in the solution of a growth crucible under microgravity conditions. The simulation model considers a simple crucible of electroepitaxy, and assumes crucible rotation and applied axial static magnetic fields to control and minimize the effect of g-jitter induced flow oscillations.

keyword: G-jitter , Microgravity , Electroepitaxy.

1 Introduction

The microgravity environment has been considered in crystal growth to minimize the adverse effects of gravity. A number of experimental and modeling studies have been carried out using various crystal growth techniques. For instance, the growth of crystals by Floating Zone (FZ) [Campbell, Schweizer, Dold, Croll and Benz (2001); Lan and Yeh (2005); Lappa (2005)], Traveling Heater Method (THM) [Lent, Dost, Redden, and Liu (2002); Jaber and Saghir (2006)], and Liquid Phase Electroepitaxy (LPEE) [Dost (1996); Kumagawa, Witt, Lichtensteiger and Gatos (1973)] has been considered under microgravity conditions.

In crystal growth from metallic solutions, the fluid flow, temperature, and concentration fields in the solution play a significant role, and affect the quality of grown crystals. It is therefore essential to have a good understanding for these transport structures and the related phenomena. From this point of view, a number of numerical simulation studies have been carried out [Imaishi and Kakimoto (2002); Kuhlman (1999); Lappa (2004)]. Furthermore, to minimize the effect of convection in the solution, the application of magnetic fields has also been considered [Imaishi and Kakimoto (2002); Series and Hurle (1991); Walker and Ma (2002); Kakimoto and Li (2006)]. The present article models numerically a simple LPEE growth crucible under microgravity conditions.

In LPEE [Dhanasekaran, Qhalid and Ramasamy (2001); Mouleeswaran and Dhanasekaran (2001); Dost, Liu and Lent (2002); Liu, Okano and Dost (2002), Sheibani, Dost, Sakai and Lent (2003); Dost, Lent, Sheibani and Liu (2004); Liu, Zytkiewicz and Dost (2004); Dost, Sheibani, Liu, Lent (2005); Khenner and Braun (2005)], growth is achieved by passing an electric current through a substrate-solution-source system under a uniform and constant furnace temperature. Thus, the temperature gradients in the system are only due to the Joule heating in the crystal and source and the Peltier heating/cooling at the growth and dissolution interfaces, and are very small. The applied electric current is the only driving force for growth, and the growth rate is almost proportional to the electric current density. This provides a great controllability for the growth rate and leads to a superior crystal composition uniformity [Dost, Shebani, and Lent (2003)]. In addition, the growth temperature is relatively low compared with the melt growth systems, and therefore, the grown crystals may have less thermal stresses. For a detailed account of LPEE, the reader is referred to [Dost and Lent (2007)] and the references therein.

The microgravity environment such as the international space station (ISS) seems to be a feasible platform for the growth of high quality crystals, due to the absence of strong natural convection. However, a growth platform in the ISS may subject to steady and periodic vibrations (the so-called g-jitter) due to equipment and crew movements and fluctuations in the gravity level. Such vibrations can lead to three-dimensional unsteady flow and growth striations in the solution/melt of a crystal growth set up [Benz and Dold (2002); Okano, Umemura and Dost (2001); Yan, Shevtsova and Saghir (2005); Semma, Ganaoui, Timchenko and Leonardi (2006)]. Therefore, even in the microgravity environment where the gravitational force is weak, such vibrations may play a signif-

[1] Shizuoka University, Hamamatsu, Shizuoka, Japan
[2] Crystal Growth Laboratory, University of Victoria, Victoria, BC, Canada

icant role, and the understanding and the control of the effect of g-jitter is essential.

A feasible option to control such vibrations is the use of an applied magnetic field. Indeed, the application of an applied magnetic field in the microgravity environment has been investigated numerically in a vertical Bridgman crucible by [Yeckel and Derby (2004)], and their results showed that a magnetic field is effective in damping the g-jitter induced fluid flow in the melt, and reducing its effect on the concentration field.

This article presents the results of a numerical simulation study that was carried out to examine the effect of g-jitter on the flow and concentration structures observed in the solution of a growth crucible under microgravity conditions. The simulation model considers a generic, simple LPEE crucible which is assumed to be subject to a crucible rotation and an applied axial static magnetic field in order to control and minimize the effect of g-jitter. The numerical simulation results show that the convective flow in the solution is stronger when the g-jitter is perpendicular to the growth direction and the magnitude of flow oscillations is larger at the lower g-jitter frequency levels. The application of a static magnetic field of 0.24 T does not provide the desired suppression in the solution. However, it seems the application of a crucible rotation is very effective in suppressing the g-jitter induced flow oscillations in the solution, even at a very low rate of 10 rpm.

2 Numerical method

2.1 Governing equations

The LPEE set up modeled is a simple system which consists of a CdZnTe single crystal substrate at the bottom, a Cd-Zn-Te solvent (solution) in the middle, and a polycrystalline CdZnTe source at the top. ZnTe was assumed to be as the solute in the solution. A schematic view of the computational domain is shown in Fig.1. In the model, the growth cell is 70 mm in height and 100 mm in diameter, and the substrate and the source are of 10 mm thickness. For simplicity, the crucible and its other components were not included in the model, and the solid/liquid interfaces were assumed remain flat. The applied electric current passes through the set up uniformly. The initial temperature was set at 1083 K.

Due to the inclusion of crucible rotation, the time-dependent three-dimensional rotational coordinate system was used. In this system, the governing equations in the liquid phase are the continuity, momentum, energy, mass transport and the electric charge balance equations, which are given respectively as

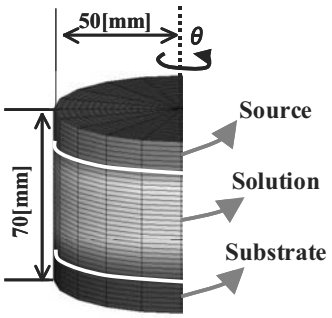

Figure 1 : Schematic view of the computational domain.

Continuity:

$$\frac{1}{r}\left(\frac{\partial(ru)}{\partial r}+\frac{\partial(rv)}{\partial z}+\frac{\partial w}{\partial\theta}\right)=0 \tag{1}$$

Momentum:

$$\begin{aligned}&\frac{\partial u}{\partial t}+u\frac{\partial u}{\partial r}+v\frac{\partial u}{\partial z}+\frac{w}{r}\frac{\partial u}{\partial\theta}-\frac{w^2}{r}\\&\quad=-\frac{1}{\rho}\frac{\partial p}{\partial r}\\&\quad+\nu\left(\frac{\partial}{\partial r}\left(\frac{1}{r}\frac{\partial(ru)}{\partial r}\right)+\frac{\partial^2 u}{\partial z^2}+\frac{1}{r^2}\frac{\partial^2 u}{\partial\theta^2}-\frac{2}{r^2}\frac{\partial w}{\partial\theta}\right)\\&\quad+\left(g+\omega^2 r\right)\left(\beta_t\Delta T+\beta_c\Delta C\right)-2\omega w+\frac{1}{\rho}F_r\end{aligned} \tag{2}$$

$$\begin{aligned}&\frac{\partial v}{\partial t}+u\frac{\partial v}{\partial r}+v\frac{\partial v}{\partial z}+\frac{w}{r}\frac{\partial v}{\partial\theta}\\&\quad=-\frac{1}{\rho}\frac{\partial p}{\partial z}+\nu\left(\frac{1}{r}\frac{\partial}{\partial r}\left(r\frac{\partial v}{\partial r}\right)+\frac{\partial^2 v}{\partial z^2}+\frac{1}{r^2}\frac{\partial^2 v}{\partial\theta^2}\right)\\&\quad+g\left(\beta_t\Delta T+\beta_c\Delta C\right)+\frac{1}{\rho}F_z\end{aligned} \tag{3}$$

$$\begin{aligned}&\frac{\partial w}{\partial t}+u\frac{\partial w}{\partial r}+v\frac{\partial w}{\partial z}+\frac{w}{r}\frac{\partial w}{\partial\theta}+\frac{uw}{r}\\&\quad=-\frac{1}{r\rho}\frac{\partial p}{\partial\theta}\\&\quad+\nu\left(\frac{\partial}{\partial r}\left(\frac{1}{r}\frac{\partial(rw)}{\partial r}\right)+\frac{\partial^2 w}{\partial z^2}+\frac{1}{r^2}\frac{\partial^2 w}{\partial\theta^2}+\frac{2}{r^2}\frac{\partial u}{\partial\theta}\right)\\&\quad+g\left(\beta_t\Delta T+\beta_c\Delta C\right)+2\omega u+\frac{1}{\rho}F_\theta\end{aligned} \tag{4}$$

Energy:

$$\frac{\partial T}{\partial t}+u\frac{\partial T}{\partial r}+v\frac{\partial T}{\partial z}+\frac{w}{r}\frac{\partial T}{\partial \theta} = \alpha\left(\frac{1}{r}\frac{\partial}{\partial r}\left(r\frac{\partial T}{\partial r}\right)+\frac{\partial^2 T}{\partial z^2}+\frac{1}{r^2}\frac{\partial^2 T}{\partial \theta^2}\right) \quad (5)$$

Mass transport:

$$\frac{\partial c}{\partial t}+u\frac{\partial c}{\partial r}+v\frac{\partial c}{\partial z}+\frac{w}{r}\frac{\partial c}{\partial \theta}+\mu E_z\frac{\partial c}{\partial z} = D\left(\frac{1}{r}\frac{\partial}{\partial r}\left(r\frac{\partial c}{\partial r}\right)+\frac{\partial}{\partial z}\left(\frac{\partial c}{\partial z}\right)+\frac{1}{r^2}\frac{\partial^2 c}{\partial \theta^2}\right) \quad (6)$$

Electric charge:

$$\frac{\partial^2 \phi}{\partial r^2}+\frac{1}{r}\frac{\partial \phi}{\partial r}+\frac{\partial^2 \phi}{\partial z^2}+\frac{1}{r^2}\frac{\partial^2 \phi}{\partial \theta^2}=0 \quad (7)$$

with

$$E_r=-\frac{\partial \phi}{\partial r}, E_z=-\frac{\partial \phi}{\partial z}, E_\theta=-\frac{1}{r}\frac{\partial \phi}{\partial \theta} \quad (8)$$

where u, v and w are, respectively, the velocity components in the radial (r), vertical (z), and azimuthal (θ) directions, t is time, p is pressure, T is temperature, c is the ZnTe concentration in the Cd-Zn-Te solution, ρ is the solution density, β_t and β_c denote, respectively, the thermal and solutal expansion coefficients, g is the gravitational acceleration vector, α is the thermal diffusivity, and ν is kinetic viscosity. μ and D denote, respectively, the solute mobility and the diffusion coefficient in the solution. ω is crucible rotation rate. F_r, F_z and F_θ are the magnetic body force components along the r, z and θ directions, respectively. These magnetic force components are introduced in detail in the next section. E_r, E_z and E_θ are the electric field intensities in the r, z and θ directions, which are obtained by solving an axisymmetric quasi-steady electric field (ϕ) equation.

The governing equations were discretized by Finite Volume Method and solved by SIMPLE algorithm [Patankar (1980)].

The QUICK scheme [Leonard (1979)] was applied to descretize the convective terms in the governing equations. The Prandtl (Pr=ν/α) and Schmidt numbers (Sc=ν/D) of the liquid are estimated as 0.406 and 41.1, respectively.

The residual acceleration experienced by the space craft under microgravity is composed of a steady acceleration component (residual gravity: $\boldsymbol{G}$) and a time-dependent acceleration component (g-jitter: $\boldsymbol{g}_j$). The amplitude of the time-dependent component is much larger than that of the steady component. The real g-jitter data can be taken from the space flight experiments, but the following gravity modulation was applied in this study for simplicity;

$$g_j = 0.5 g_{am}\{\sin(2\pi\Omega t-\frac{\pi}{2})+1\} \quad (9)$$

where g_{am} is the amplitude of the gravity modulation, and assumed to be 10^{-4} g_0 and Ω and t are the frequency and time, respectively. The total gravity g is represented as follow;

$$g = G + g_j \quad (10)$$

The residual gravity, G, is set to be $10^{-6} g_0$ (g_0 =9.8[m^2/s]).

The boundary conditions of the model are follows:

Along the vertical boundary:

$$u=v=w=0,\quad T=T_g-\left(\frac{z-z_0}{H}\right)\Delta T, \frac{\partial \phi}{\partial r}=0, \frac{\partial c}{\partial r}=0 \quad (11)$$

Along the growth interface:

$$u=v=w=0,\quad k_s\frac{\partial T}{\partial z}-k_l\frac{\partial T}{\partial z}=-\pi J, -\sigma\frac{\partial \phi}{\partial z}=J, c=c_1 \quad (12)$$

Along the dissolution interface:

$$u=v=w=0,\quad k_s\frac{\partial T}{\partial z}-k_l\frac{\partial T}{\partial z}=+\pi J, \phi=0, c=c_2 \quad (13)$$

In the above equations, π is the Peltier coefficient, J is the applied electric current density, σ is the electrical conductivity of the liquid, H is the height of the solution zone, k_s and k_l are the thermal conductivities of the solid and liquid phases, respectively. c_1 and c_2 are the solution concentrations at the growth and dissolution interfaces, respectively. T_g is growth temperature. ΔT is used to denote the temperature drop due to the heat loss when heat is transferred from the outside wall of the furnace to the

vertical wall of the cell. It was assumed that the contribution of latent heat is negligible since the growth rate is slow.

In the solid phase, i.e. the substrate and source, the heat conduction equation was solved.

2.2 Magnetic body force components

The applied static magnetic field is assumed to be either along the growth direction or perpendicular, as

Vertical

$$\boldsymbol{B} = \begin{pmatrix} B_r \\ B_z \\ B_\theta \end{pmatrix} = B_0 \begin{pmatrix} 0 \\ 1 \\ 0 \end{pmatrix} \tag{14}$$

Horizontal

$$\boldsymbol{B} = \begin{pmatrix} B_r \\ B_z \\ B_\theta \end{pmatrix} = B_0 \begin{pmatrix} \cos\theta \\ 0 \\ -\sin\theta \end{pmatrix} \tag{15}$$

where $\boldsymbol{B}$ is the applied magnetic field with field intensity B_0. The magnetic body force acting on the points of the metallic liquid solution is then expressed by

$$\boldsymbol{F} = \boldsymbol{J} \times \boldsymbol{B} \tag{16}$$

and the current density $\boldsymbol{J}$ is assumed to be given by Ohm's law as follows:

$$\boldsymbol{J} = \sigma_e \left(\boldsymbol{E} + \boldsymbol{V} \times \boldsymbol{B}\right) \tag{17}$$

where $\boldsymbol{E}$ and $\boldsymbol{V}$ represent, respectively, the electrical field and velocity vectors acting on fluid points. The induced electric field due to the applied magnetic field and the fluid motion was neglected since the induced electric field is small.

The solution of Eq.(7) lead to the following expression for $\boldsymbol{E}$:

$$\boldsymbol{E} = \begin{pmatrix} E_r \\ E_z \\ E_\theta \end{pmatrix} = \begin{pmatrix} 0 \\ -\frac{\partial \phi}{\partial z} \\ 0 \end{pmatrix} \tag{18}$$

Eq(18) shows that the electric field intensity is zero along the $r-$ and θ- directions, and is constant along the $z-$direction. The electric current density in Eq.(17) and Lorentz force in Eq.(16) are described as follows:

Vertical

$$\boldsymbol{J} = \begin{pmatrix} J_r \\ J_z \\ J_\theta \end{pmatrix} = \sigma_e \begin{pmatrix} -wB_z \\ -\frac{\partial \phi}{\partial z} \\ uB_z \end{pmatrix} \tag{19}$$

$$\boldsymbol{F} = \begin{pmatrix} F_r \\ F_z \\ F_\theta \end{pmatrix} = \begin{pmatrix} -J_\theta B_z \\ 0 \\ J_r B_z \end{pmatrix} \tag{20}$$

Horizontal

$$\boldsymbol{J} = \begin{pmatrix} J_r \\ J_z \\ J_\theta \end{pmatrix} = \sigma_e \begin{pmatrix} vB_\theta \\ -\frac{\partial \phi}{\partial z} + wB_r - uB_\theta \\ -vB_r \end{pmatrix} \tag{21}$$

$$\boldsymbol{F} = \begin{pmatrix} F_r \\ F_z \\ F_\theta \end{pmatrix} = \begin{pmatrix} J_z B_\theta \\ J_\theta B_r - J_r B_\theta \\ -J_z B_r \end{pmatrix} \tag{22}$$

The following assumptions were made in the analysis:

1. Boussinesq approximation holds.
2. The electric field is aligned with the symmetry axis of the growth crucible.
3. The electric and magnetic fields are constant and uniform.

The contribution of Joule heating in the liquid zone is neglected since the liquid Cd-Zn-Te solution is a good conductor.

3 Results and discussion

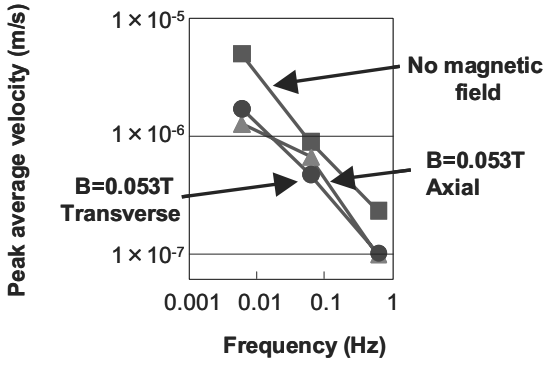

Figure 2 : Validity of the simulation code—comparison with the results by Yackel and Derby (2004).

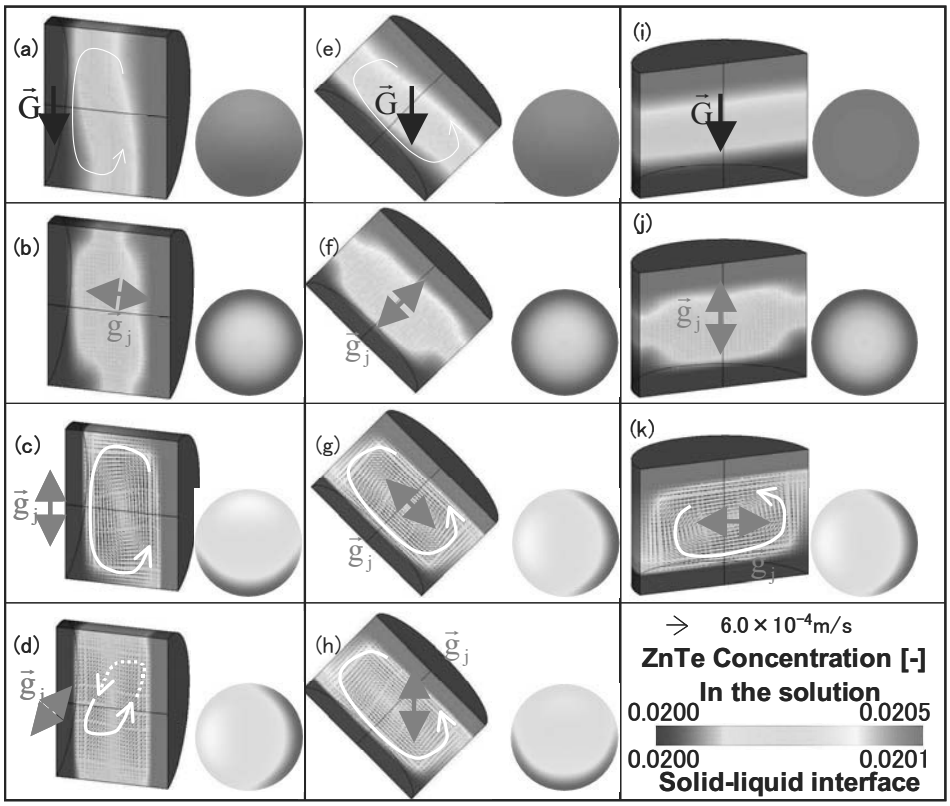

Figure 3 : The effect of g-jitter direction on the flow (vector) and concentration (color) fields. Left figures: flow and concentration fields in the vertical plane. Black, red and white arrows show the directions of residual gravity, g-jitter, and flow, respectively. Right figures: the concentration fields in the solution near the seed/solution interface.

The simulation domain shown in Fig.1 was divided into 40 (r) x 40 (θ) x 70 (z) after examining its mesh dependency. The code used here was first verified by comparing the results with those of [Yackel and Derby (2004)], as shown in Fig.2. In this figure, the lines describe the results of [Yackel and Derby (2004)], and the symbols (full circles, triangles, and squares) represent the results obtained using our simulation code. The agreement between these results is reasonably good as seen from Fig.2.

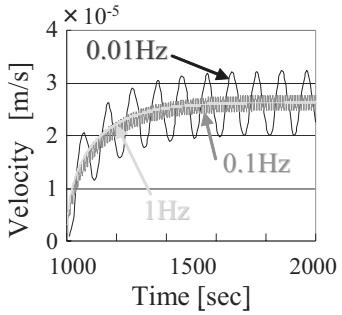

Figure 4 : The effect of g-jitter frequency on induced velocity in the vicinity of solid-liquid interface.

3.1 Influence of g-jitter direction and frequency

Fig.3 presents the computed results for the flow (vector) and concentration field (color) at the g-jitter frequency of 0.01 Hz. In each frame, the left figure describes the flow and concentration fields in the vertical plane, and the right figure represents the concentration distribution in the solution near the growth interface (the seed/solution interface). The simulation results in the absence of g-jitter are given in Fig.3 (a), (e) and (i) for comparison.

The simulation results show that when the g-jitter is perpendicular to the growth direction (Fig.3 (c), (d), (g) and (k)), in other words, acts in the radial plane, the concentration distribution along the growth interface becomes non-uniform and asymmetric. This can be attributed to the strong convection observed in this case. On the other hand, when the g-jitter acts along the growth direction,

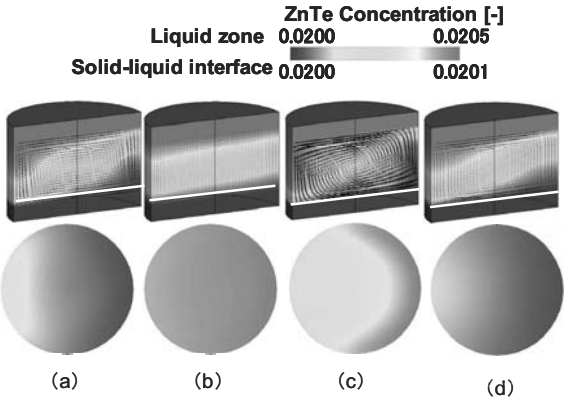

Figure 5 : The effect of applied vertical and horizontal magnetic fields on concentration distribution in the liquid and along the growth interface when g-jitter frequency is 0.01 Hz. (a) vertical Ha=46 [0.1 T], (b) vertical Ha=115 [0.25T], (c) horizontal Ha=46 [0.1 T] and (d) horizontal Ha=115 [0.25T].

its effect on convection is not notable numerically (see Fig.3 (b), (f) and (j)).

The effect of the g-jitter frequency on fluid flow velocity near the growth interface (at the centre and 0.5 mm away from the growth interface) is presented in Fig.4 for the case considered in Fig.3 (k). As seen, the flow velocity is affected by the frequency. Lower frequencies induce velocity fluctuations with larger amplitude. For the present set up considered in this work, the frequency levels lower than 0.1 Hz may lead to growth striations in the grown crystal.

3.2 Control of flow fluctuations by crucible rotation and magnetic fields

As shown in the previous section, g-jitter induces fluctuations in the flow field in the solution. Especially, the g-jitter with low frequencies acting in the radial plane (perpendicular to the growth direction) induces large-amplitude velocity fluctuations. Such flow fluctuations must be suppressed and controlled in order to minimize their adverse effects on the crystal quality. To this end, one may consider two possible options: (1) the rotation of the growth crucible, and (2) the use of an applied magnetic field.

The body forces exerted by a crucible rotation (centrifugal and Coriolis forces) and by an applied magnetic field (magnetic body forces) acting on the points

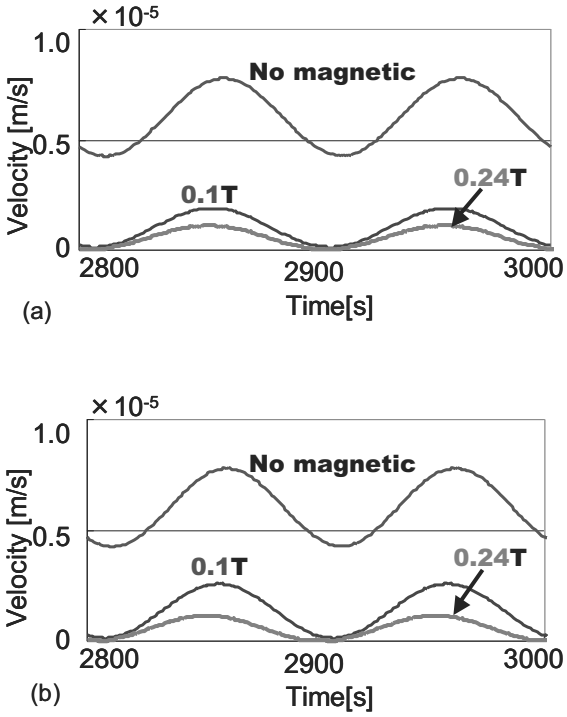

Figure 6 : The effect of magnetic field application on the flow velocity when g-jitter frequency is 0.01 Hz. (a) vertical field and (b) horizontal field.

of the solution balance the effect of the gravitational body force, and thereby suppress convection and flow fluctuations. The effectiveness of a crucible rotation in suppressing convection in crystal growth is known [see, for instance, Okano, Kondo and Dost (2002); Okano, Nishino, Ohkubo and Dost (2002)]. The use of applied magnetic fields in crystal is widely considered, and the literature in this area is relatively rich [the literature for solution growth see Dost and Lent (2007), and for the melt growth see Hurle and Series (1994)]. In this work we consider both options.

3.2.1 Applied vertical and horizontal magnetic fields

The simulation results on the effect of vertical and horizontal magnetic fields are presented in this section. The computed flow field and the solute concentration distribution for the case considered in Fig.3 (k) are presented in Fig.5. In Fig.5, *Ha* represents the Hartman number defined as $(\sigma/\mu)^{1/2}B_0L$ where L is radius of the cylinder. The results under the effect of a vertical magnetic field (along the growth direction) are shown in Fig.5 (a) and (b), and those under an horizontal magnetic field (per-

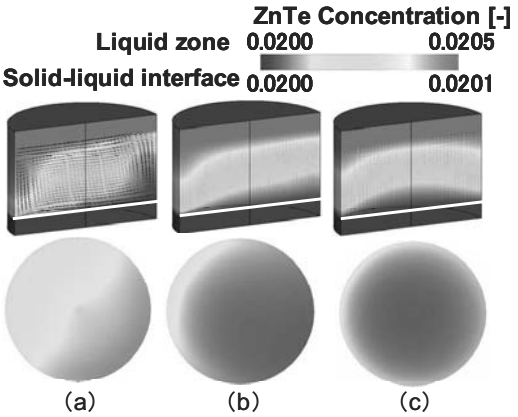

Figure 7 : The effect of crucible rotation rate on concentration distribution in the liquid, along the growth interface when g-jitter frequency is 0.01 Hz. (a) 1 rpm, (b) 3 rpm and (c) 10 rpm.

pendicular to the growth direction) in Fig.5 (c) and (d). The time dependency of the velocity field at the center near the growth interface (0.5 mm from the growth interface) is presented in Fig.6 (a) for the vertical magnetic field, and in Fig.6 (b) for the horizontal field.

As can be seen from these figures, the concentration distribution along growth interface becomes uniform with the increasing magnetic field intensity. The flow velocity is also suppressed significantly by the application of magnetic fields. However, as seen in Fig.6 (a) and (b), the flow fluctuations become smaller, but still remain. Therefore, larger magnetic fields may be necessary to suppress the flow fluctuations further.

3.2.2 Crucible rotation

The results for the flow field and solute concentration distribution for crucible rotation rates of (a) 1 rpm, (b) 3 rpm and (c) 10 rpm are shown in Fig.7. As seen, the flow field is significantly suppressed at a rotation rate of 10 rpm, and the concentration field becomes more symmetric.

The time dependency of the velocity field at the same point, at the center 0.5 mm above the growth interface, is given in Fig.8. As can be seen, the flow fluctuations are almost eliminated at a 10 rpm crucible rotation rate, although the flow field is not fully suppressed. The concentration distribution becomes uniform with the increasing rotation rate.

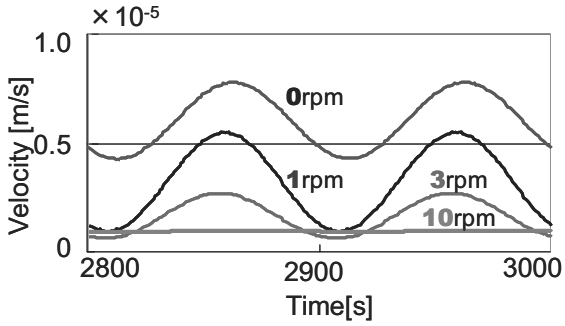

Figure 8 : The effect of crucible rotation on flow velocity when g-jitter frequency is 0.01 Hz.

4 Conclusions

A numerical simulation study was carried out to examine the effect of g-jitter on the flow and concentration structures observed in the solution of a growth crucible under microgravity conditions. The simulation results show that the convective flow in the solution is stronger when the g-jitter is perpendicular to the growth direction and the magnitude of flow oscillations is larger at the lower g-jitter frequency levels. The application of a static magnetic field (up to a field intensity of 0.24 T) does not provide the desired suppression in the solution. Stronger field levels may be necessary. However, a low crucible rotation rate (at 10 rpm) seems very effective in suppressing the g-jitter induced flow fluctuations in the solution.

References

Benz, K. W.; Dold, P. (2002): Crystal growth under microgravity: present results and future prospects towards the International Space Station. *J. Crystal Growth*, vol. 237-239, pp.1638-1645.

Campbell, T. A.; Schweizer, M.; Dold, P.; Croll, A.; Benz, K. W. (2001) Float zone growth and characterization of $Ge_{1-x}Si_x$ (x<10at %) single crystal. *J. Crystal Growth*, vol. 226, pp.231-239.

Dhanasekaran, R.; Qhalid, R. S.; Ramasamy, P. (2001): Simulation studies on the liquid phase electroepitaxial growth of III-V compound semiconductors. *J. Crystal Growth*, vol. 229, pp. 169-174.

Dost, S. (1996): Recent developments in modeling of liquid phase electroepitaxy: A continuum approach. *Appl. Mech. Rev.*, vol. 49, pp.477-495.

Dost, S.; Liu, Y.; Lent, B. (2002): A numerical simulation study for the effect of applied magnetic field in liquid phase electroepitaxy. *J. Crystal Growth*, vol. 240, pp. 39-51.

Dost, S.; Lent, B.; Sheibani, H.; Liu, Y. C. (2004): Recent developments in Liquid Phase Electroepitaxial growth of bulk crystals under magnetic field. *Comptes Rendus Mecanique*, vol. 332, pp. 413-428.

Dost, S.; Sheibani, H.; Liu, Y. C.; Lent, B. (2005): On the high growth rates in electroepitaxial growth of bulk semiconductor crystals in magnetic field. *J. Crystal Growth*, vol. 275, pp. e1-e6.

Dost, S.; Lent, B. (2007): *Single Crystal Growth of Semiconductors from Metallic Solutions*, Elsevier, Holland.

Hurle, D. T. J.; Series, R. W. (1994): Use of magnetic field in melt growth. *Handbook of crystal growth*, vol. 2, pp. 261-285.

Imaishi, N.; Kakimoto, K. (2002): Convective instability in crystal growth system. *Annual Rev. Heat Transfer*, vol. 12, pp. 187-221.

Jaber, T. J.; Saghir, M. Z. (2006): The Effect of Rotating Magnetic Fields on the Growth of SiGe Using the Traveling Solvent Method. *FDMP: Fluid Dynamics and Materials Processing*, vol. 2, no. 3: pp. 175-190 to appear

Kakimoto, K.; Liu, L. (2006): Flow instability of silicon melt in magnetic fields. *FDMP: Fluid Dynamics and Materials Processing*, vol. 2, no. 3: pp. 167-174 to appear

Khenner, M.; Braun, R. J. (2005): Numerical simulation of liquid phase electro-epitaxial selective area growth. *J. Crystal Growth*, vol. 279, pp. 213-228.

Kuhlmann, H. C. (1999): *Thermocapillary convection in models of crystal growth. Springer Tracks in Modern Physics*, vol. 152, Springer-Verlag Berlin Heidelberg.

Kumagawa, M.; Witt, A. F.; Lichtensteiger, M.; Gatos, H. C. (1973): Current-controlled growth and dopant modulation in liquid phase epitaxy. *J. Electrochem. Soc.*, vol. 120, pp. 583-584.

Lan C. W.; Yeh B.C., (2005): Effects of rotation on heat flow, segregation, and zone shape in a small-scale floating-zone silicon growth under axial and transversal magnetic fields. *FDMP: Fluid Dynamics and Materials Processing*, vol. 1, no. 1, pp. 33-44.

Lappa, M. (2004): *Fluids, Materials and Microgravity. Numerical Techniques and Insights into the Physics, Elsevier.*

Lappa, M. (2005): Review: Possible strategies for the control and stabilization of Marangoni flow in laterally heated floating zones. *FDMP: Fluid Dynamics and Materials Processing*, vol. 1, no.2, pp. 171-188.

Lent, B.; Dost, S.; Redden, R. F.; Liu, Y. (2002): Mathematical simulation of the traveling heater method growth of ternary semiconductor materials under suppressed gravity conditions. *J. Crystal Growth*, vol. 237-239, pp. 1876-18801.

Leonard, B. P. (1979): A stable accurate convective modeling procedure based on quadratic upstream interpolation. *Comp. Meth. Appl. Mech. Eng.*, vol. 19, pp. 59-98.

Liu, Y. C.; Okano, Y.; Dost, S. (2002): The effect of applied magnetic field on flow structures in liquid phase electroepitaxy—a three-dimensional simulation model. *J. Crystal Growth*, vol. 244, pp. 12-26.

Liu, Y. C.; Zytkiewicz, Z. R.; Dost, S. (2004): A model for epotaxial lateral overgrowth of GaAs by liquid-phase electroepitaxy. *J. Crystal Growth*, vol. 265, pp. 341-350.

Mouleeswaran, D.; Dhanasekaran, R. (2001): Investigations on liquid phase kinetics of GaAs. *Mater. Sci. Eng. B*, vol. 112 pp. 91-95.

Okano, Y.; Kondo, H.; Dost, S. (2002): Numerical study of interface shape control in the VGF growth of compound semiconductor crystal. *J. Crystal Growth*, vol. 237-239, pp.1769-1772.

Okano, Y.; Nishino, S.; Ohkubo, S.; Dost, S. (2002): Numerical study of transport phenomena in the THM growth of compound semiconductor crystal. *J. Crystal Growth*, vol. 237-239, pp. 1779-1784.

Okano, Y.; Umemura, S.; Dost, S. (2001): G-jitter effect on the flow in a Three-Dimensional Rectangular Cavity. *J. Mater. Processing Manufacturing Sci.*, vol. 10, pp. 3-6.

Patankar, S. V. (1980): Numerical heat transfer and fluid flow, *Washington*.

Semma, E.A.; El Ganaoui, M.; Timchenko, V.; Leonardi, E. (2006): Some Thermal Modulation Effects on Directional Solidification. *FDMP: Fluid Dynamics and Materials Processing*, vol. 2, no. 3: pp. 191-202 to appear

Series, R. W.; Hurle, D. T. J. (1991): The use of magnetic fields in semiconductor crystal growth. *J. Crystal Growth*, vol. 113, pp. 305-328.

Sheibani, H.; Dost, S.; Sakai, S.; Lent, B. (2003): Growth of bulk single crystals under applied magnetic field liquid phase electroepitaxy. *J. Crystal Growth*, vol. 258, pp. 283-295.

Yan, Y.; Shevtsova, V.; Saghir, M.Z. (2005): Numerical study of low frequency g-jitter effect on thermal diffusion. *FDMP: Fluid Dynamics and Materials Processing*, vol. 1, no. 4, pp. 315-328.

Yeckel, A.; Derby, J. J. (2004): Dynamics of three-dimensional convection in microgravity crystal growth: g-jitter with steady magnetic fields. *J. Crystal Growth*, vol. 263, pp. 40-52.

Walker, J. S.; Ma, N. (2002): Convective mass transfer during bulk growth of semiconductor crystals with steady magnetic fields. *Annual Rev. Heat Transfer*, vol. 12, pp. 223-263.